Shock-Induced Chemical Changes in Neat Nitromethane: Use of Time-Resolved Raman Spectroscopy

J. M. Winey and Y. M. Gupta*

Shock Dynamics Center and Department of Physics Washington State University, Pullman, Washington 99164-2814

Received: August 7, 1997; In Final Form: October 8, 1997[⊗]

Time-resolved Raman spectroscopy was used to examine chemical changes in neat liquid nitromethane subjected to stepwise loading to peak pressures of 14−17 GPa. After a peak pressure at 14 GPa was reached, no changes in the CN (917 cm^{-1}), NO_2 (1400 cm^{-1}), and CH_3 (2968 cm^{-1}) symmetric stretching modes were observed. After a peak pressure at 16 GPa was reached, time-dependent changes were observed during the induction period reported in previous absorption experiments. At this peak pressure, the extent of reaction was small, and the observed changes in the CH_3 and CN modes indicated prereaction changes in the sample bulk. After a peak pressure at 17 GPa was reached (980 K peak temperature), all three peaks disappeared, indicating that the extent of reaction was substantial under these conditions. The broadening of the CH_3 peak and the softening of the CN mode observed in this work suggest strong intermolecular interactions. These interactions lead to a reaction precursor involving proposed head-to-tail intermolecular associations with decomposition proposed to follow through a bimolecular reaction, put forward by Bardo, which forms nitrosomethane and nitromethanol. Confirmation of these ideas will require different spectroscopic methods, since Raman measurements are primarily useful for probing initial changes in the sample.

I. Introduction

Shock wave-induced decomposition of liquid nitromethane (NM), a prototypical energetic material, has been the subject of many previous investigations.[1] Most of these studies have examined the reaction kinetics through the use of continuum measurements.[1−6] However, the determination and understanding of the reaction mechanisms involved in shock-induced decomposition of NM is an important need.[7] Toward this objective, time-resolved optical spectroscopy methods have been used to probe molecular level changes in shocked NM. Time-resolved Raman and UV−vis absorption measurements were performed on samples of neat NM[8,9] and mixtures of NM and ethylenediamine (EDA),[9,10] subjected to stepwise loading up to 14 GPa. These experiments yielded mechanistic information on the shock-induced reaction in NM/EDA mixtures. However, no evidence of shock-induced decomposition in neat NM was observed at these pressures.

Recently, changes in the UV−vis absorption spectra, indicative of a shock-induced reaction, were observed in stepwise-loaded neat NM at pressures ranging from 14 to 19 GPa.[11] Similar to the continuum measurements,[2−6] the arrival of the shock wave at the sample and the onset of reaction were separated by an induction time, during which no changes in the absorption spectra were discernible. Despite the usefulness of the absorption data as a molecular level probe of reaction, the results of these experiments did not provide a basis for identifying the operative reaction mechanisms.

The objectives of the work reported here were (1) to examine molecular changes in neat NM during the induction time in previous absorption experiments,[11] (2) to experimentally determine the nature of the first step in shock-induced decomposition in neat NM, and (3) to assess the applicability of proposed mechanistic models of decomposition in neat NM to our spectroscopic data. To meet these objectives, time-resolved Raman spectroscopy was used to examine the vibrational structure of neat NM under stepwise loading (SWL) conditions. Unlike previous Raman work on neat NM under SWL,[8] the peak pressures and temperatures reached in the experiments reported here were shown[11] to induce reaction within the time duration of the experiments.

The Raman spectrum of NM at ambient conditions has been studied in detail.[12,13] In the shock experiments reported here, only the three strongest Raman peaks were observable: the CN symmetric stretching mode (917 cm^{-1}), the NO_2 symmetric stretching mode overlapped with the CH_3 symmetric bending mode (∼1400 cm^{-1}), and the CH_3 symmetric stretching mode (2968 cm^{-1}). The NO_2 scissors mode (655 cm^{-1}) is weaker and was not well-defined once the shock entered the sample.

The next section contains a brief description of the experimental method, while the experimental results are presented in section III. In section IV, the results are discussed, and a mechanism of decomposition for neat NM is proposed. In section V, the main findings are summarized.

II. Experimental Method

All experiments described here were performed using neat nitromethane (NM) as the sample material. This chemical was supplied by Aldrich Chemical Co., Inc. with a nominal purity of 99+%. It was used as received without further purification.

The experimental configuration used in this work was nearly identical with that used previously.[8] Therefore, except for new features, only a brief description of these experiments will be given. Details can be found elsewhere.[14]

A. Overall Configuration. Figure 1 gives a schematic view of the overall experimental configuration. Light (ω_0) from a pulsed dye laser (Cynosure SLL-5000, 514.5 nm, 3 μs pulse length) was delivered to the sample via an optical fiber. Typically, ∼140 mJ of laser energy was focused into a 1 mm diameter spot. The back-scattered light was delivered to the input of a spectrometer (Spex 500M, 0.5 m focal length), where the elastically scattered laser light (ω_0) was rejected using a holographic edge filter. After spectral dispersion by the spectrometer, the light was temporally dispersed, with 45 ns

[⊗] Abstract published in *Advance ACS Abstracts,* December 1, 1997.

S1089-5647(97)02588-1 CCC: $14.00

TABLE 1: Summary of Experimental Results

exptl no.	spectral dispersion	stretching mode under observation	sample thickness (μm)	initial temp (K)	projectile velocity (km/s)	calcd peak pressure (GPa)	calcd peak temperature (K)	calcd time to reach peak pressure (ns)
1	low	CN, NO_2, CH_3	300	298[a]	0.778	14.1	860	270
2	low	CN, NO_2, CH_3	253	298[a]	0.879	16.1	915	211
3	high	CH_3	368	298[a]	0.873	16.0	911	308
4	high	CN, NO_2	362	298[a]	0.871	15.9	910	303
5[b]	low	CN, NO_2, CH_3	212	298[a]	0.920	16.9	937	171
6	low	CN, NO_2, CH_3	250	323	0.811	14.7	923	221
7	low	CN, NO_2, CH_3	333	322	0.914	16.8	980	270

[a] Nominal value. [b] Unloading experiment.

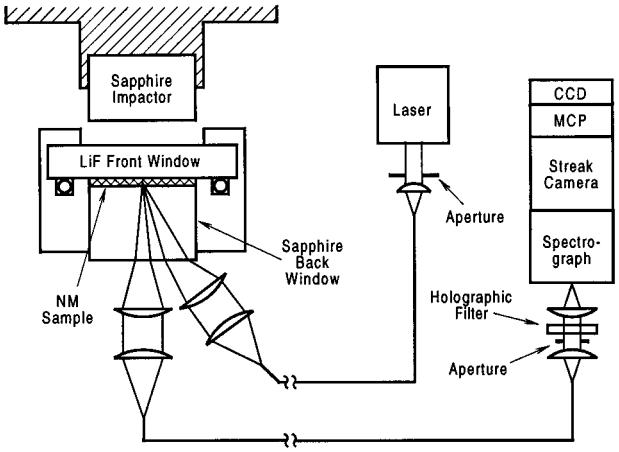

Figure 1. Schematic diagram of the experimental configuration. The pulsed laser is synchronized to provide excitation to the NM sample when the sapphire impactor drives a shock wave through the LiF front window and into the NM. The Raman-scattered light is recorded by the spectrograph−streak camera−MCP−CCD detection system. MCP, microchannel plate image intensifier. CCD, charge-coupled device.

time resolution, by an electronic streak camera. The output of the streak camera was amplified by a proximity-focused microchannel plate (MCP) image intensifier and collected with a charge-coupled device (CCD) detector (Princeton Instruments, 1024 × 1024, back-illuminated chip).

The spectrometer was used in two different configurations. In the low dispersion configuration, a 150 groove/mm ruled grating was installed, resulting in a total system band-pass of about 150 cm^{-1} at the CN stretching frequency (917 cm^{-1}) and about 120 cm^{-1} at the CH_3 stretching frequency (2968 cm^{-1}). The spectral coverage in this configuration was from approximately 500 cm^{-1} to over 3500 cm^{-1}. In the high dispersion configuration, a 600 groove/mm ruled grating was used, resulting in a total system band-pass of 43 cm^{-1} at the CN stretching frequency (917 cm^{-1}) and 34 cm^{-1} at the CH_3 stretching frequency (2968 cm^{-1}). The wavelength calibration in each of these configurations was performed using the method described in ref 8.

The sample cell, shown in Figure 1, was similar to that described earlier.[8] The liquid sample was contained between two optical windows with sample thicknesses ranging from approximately 0.20 to 0.35 mm (see Table 1). LiF front windows (38.1 mm diameter, 3.0 mm thick disk) were used instead of the sapphire windows used previously. However, sapphire was still used for the back window (25.4 mm diameter, 12.7 mm thick disk). As discussed earlier,[11,15] the effect of using a LiF front window was to increase the temperature associated with a given peak pressure state. Also, the temperature of the shocked state was raised by heating the cell prior to the shock wave experiment.[11,14]

The shock waves were generated by projectile impact, where the projectile and the sapphire impactor were accelerated to the desired velocity using a light-gas gun.[16] When the sapphire impactor (31.8 mm diameter, 15.9 mm thick disk) contacted the LiF front window of the sample cell, a plane shock wave was driven through the front window and into the NM sample. Reverberation of the shock wave between the front and back windows of the cell brought the NM sample to the peak pressure and temperature state via a stepwise loading process. The experiment was terminated when release waves from the lateral boundaries of the impactor converged in the central region of interest.

B. Calculation of Pressure and Temperature. Pressure and temperature profiles for the NM sample were calculated using the SHOCKUP[17] and COPS[18] computer codes. The peak pressure in the NM sample could be determined very accurately since it is related only to the projectile velocity and the shock response of the sapphire and LiF windows. In contrast, temperature calculations depend heavily on the equation of state (EOS) for NM. The nitromethane EOS developed in our laboratory[14,19] was described briefly in a previous publication.[11]

III. Experimental Results

Details pertinent to the time-resolved Raman experiments are summarized in Table 1. A total of seven Raman experiments are presented. Five experiments used the low dispersion configuration to examine all three symmetric stretching modes simultaneously. Experiments 3 and 4 used the high dispersion configuration to examine limited spectral ranges in more detail. The sample thickness and the projectile velocity are measured quantities. However, the peak pressure, peak temperature, and the time to reach peak pressure were all calculated using our equation of state.

A. Stepwise Loading Experiments at T_0 = 298 K. The results of experiment 1, a low dispersion experiment, are shown in Figure 2. The three peaks in the figure correspond to the CN symmetric stretching mode (917 cm^{-1}), the NO_2 symmetric stretching mode overlapped with the CH_3 symmetric bending mode (∼1400 cm^{-1}), and the CH_3 symmetric stretching mode (2968 cm^{-1}). The first set of arrows marks the spectrum that corresponds to the shock entering the sample. As seen in the figure, all three peaks shift to higher frequencies as the pressure rises in the sample. The second set of arrows marks the spectrum that corresponds to the attainment of peak pressure in the sample. After peak pressure is reached, the three peaks remain relatively constant in shape and position until the experiment terminates at about 900 ns after the shock reached the sample.

At higher pressure and temperature, spectral changes are observed after peak pressure is reached. This is seen in the results of experiment 2, shown in Figure 3. After peak pressure is reached, no major changes are observed in the three peaks until about 540 ns after the shock reached the sample. At this point, the background begins to rise rapidly and the CH_3 stretching mode shows evidence of considerable broadening, relative to the other peaks.

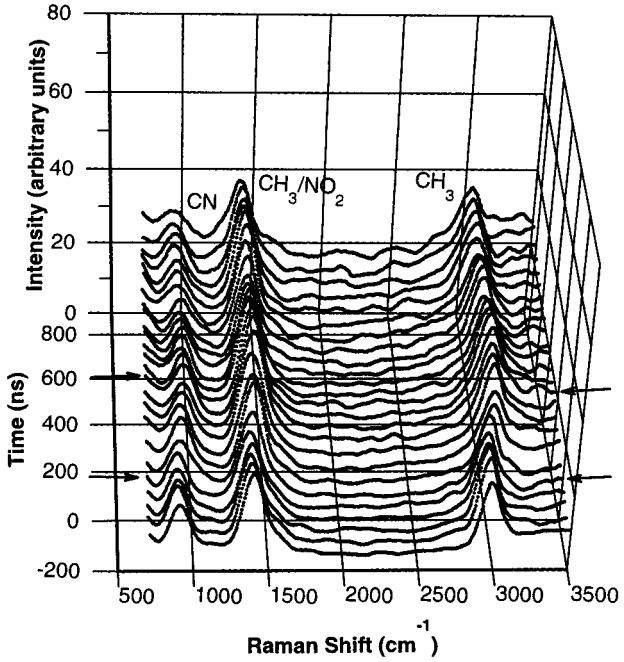

Figure 2. Raman spectra of NM shocked to 14.1 GPa (experiment 1). Peak temperature = 860 K. The times indicated are with respect to the when the shock wave reaches the sample. The time interval between spectra is 45 ns. The first set of arrows marks the spectrum where the shock entered the sample. The second set of arrows marks the spectrum where peak pressure is reached.

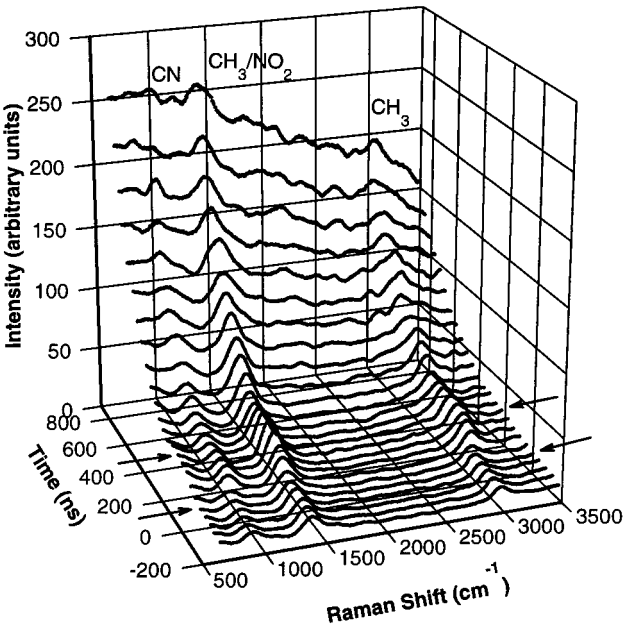

Figure 3. Raman spectra of NM shocked to 16.1 GPa (experiment 2). Peak temperature = 915 K. The times indicated are with respect to the when the shock wave reaches the sample. The time interval between spectra is 45 ns. The first set of arrows marks the spectrum where the shock entered the sample. The second set of arrows marks the spectrum where peak pressure is reached. The late changes are in marked contrast to the spectra in Figure 2.

Selected spectra from experiment 2 are shown in more detail in Figure 4. The vertical lines mark the position of the peaks prior to the arrival of the shock wave at the sample. The pressure-induced hardening of all three modes is apparent in the figure. There is also a relative enhancement of the NO_2/CH_3 mode which appears with the increase in shock pressure. Later in time, the CH_3 peak broadens to a degree that is not evident in the CN peak or NO_2/CH_3 peak.

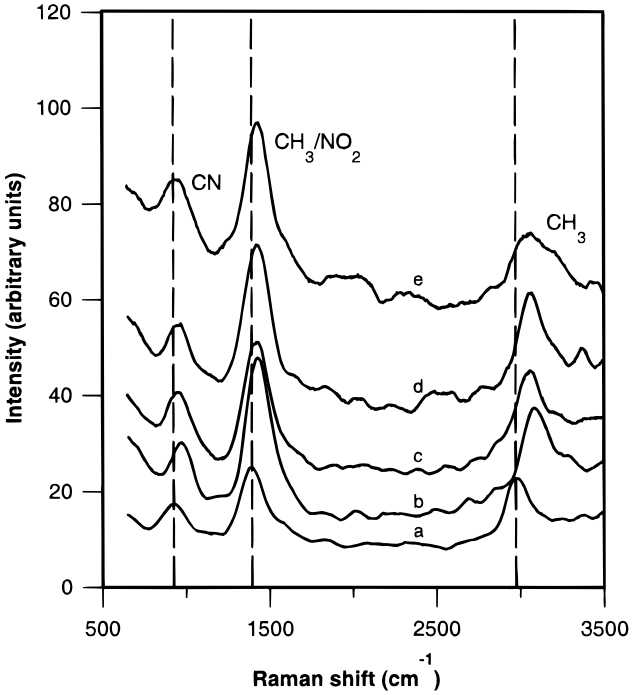

Figure 4. Selected Raman spectra of NM shocked to 16.1 GPa (experiment 2). Peak temperature = 915 K. Time relative to the when the shock wave reached the sample: (a) 0 ns, (b) 225 ns, (c) 405 ns, (d) 495 ns, (e) 585 ns. The vertical lines mark the positions of the peaks at ambient pressure. Peak pressure was attained at 211 ns.

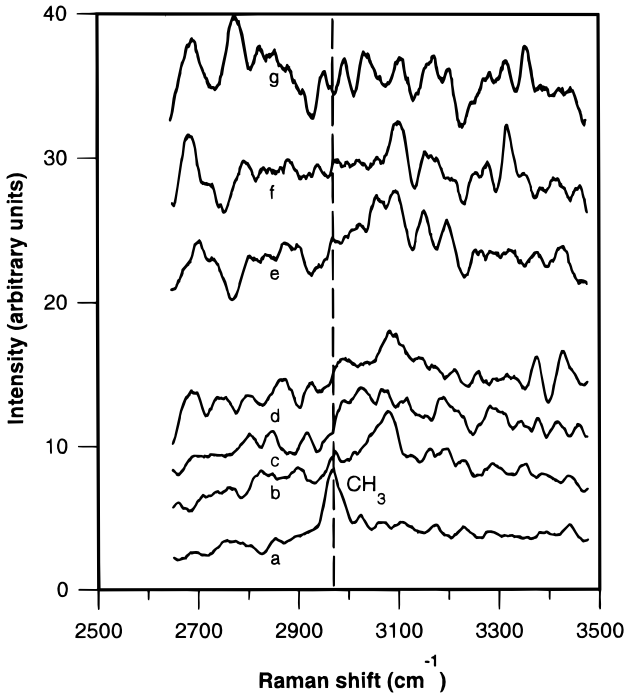

Figure 5. Selected Raman spectra of NM shocked to 16.0 GPa (experiment 3). Peak temperature = 911 K. Time relative to the when the shock wave reached the sample: (a) 0 ns, (b) 315 ns, (c) 405 ns, (d) 450 ns, (e) 540 ns, (f) 585 ns, (g) 630 ns. The vertical line marks the position of the peak at ambient pressure. Peak pressure was attained at 308 ns. Spectrum (a) has been vertically offset by −1000 units to prevent overlap of the spectra.

Experiment 3 was performed to examine the broadening of the CH_3 stretching mode using the high dispersion configuration. The results are shown in Figure 5. The noise in these spectra is due to low-level fluorescence from the sapphire back window. Despite this noise, the features of interest are still discernible. As expected, the peak shifts to higher energy as the sample

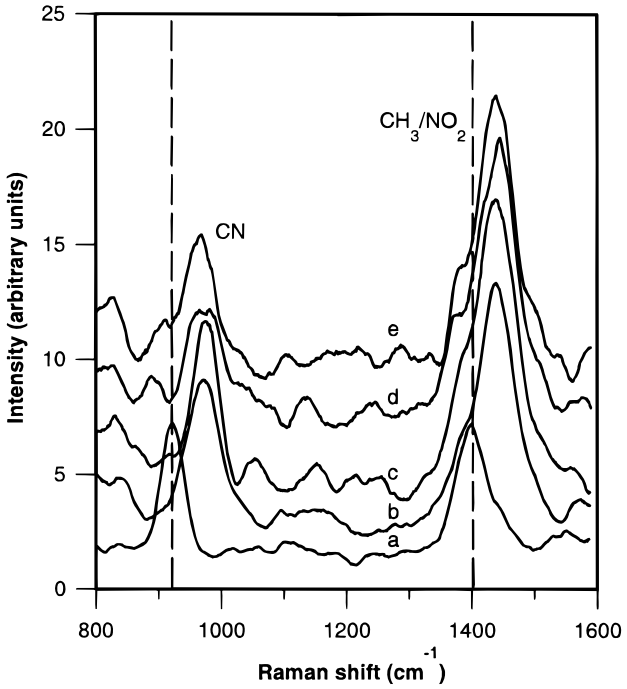

Figure 6. Selected Raman spectra of NM shocked to 15.9 GPa (experiment 4). Peak temperature = 910 K. Time relative to the when the shock wave reached the sample: (a) 0 ns, (b) 315 ns, (c) 495 ns, (d) 675 ns, (e) 765 ns. The vertical lines mark the positions of the peaks at ambient pressure. Peak pressure was attained at 303 ns. In contrast to the CH_3 mode in Figure 5, the CN and NO_2 modes exhibit little broadening after peak pressure is reached.

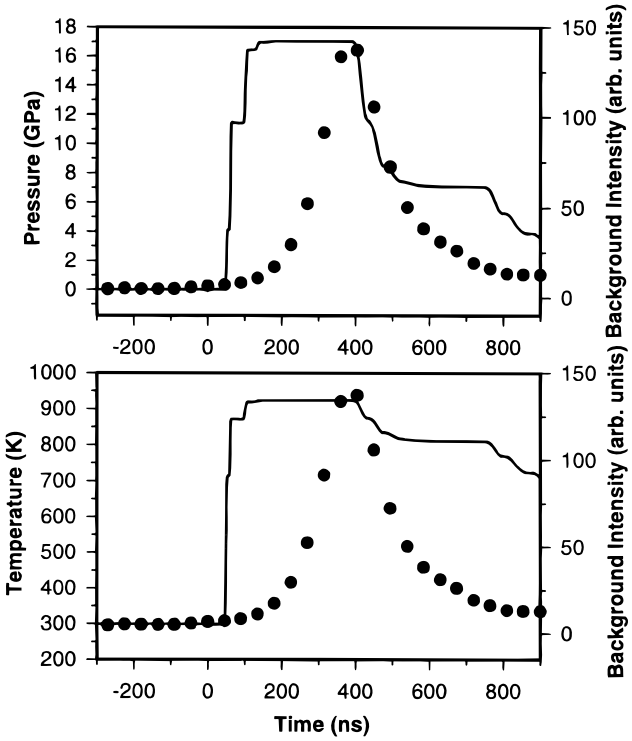

Figure 7. Comparison of pressure and temperature histories with background level history (experiment 5). Peak pressure = 16.9 GPa, peak temperature = 937 K. The solid line is the calculated[18] pressure or temperature history. The dots indicate the recorded background intensity. Time is relative to when the shock wave reached the sample. The background levels were sampled at a wavelength of 574 nm (2000 cm^{-1} in the Raman spectrum), which is far from any Raman peaks of NM.

pressure increases. Very quickly after peak pressure is reached, the CH_3 peak broadens substantially. This broadening is observed at an earlier time than was observed under low dispersion (experiment 2). Following the onset of CH_3 broadening, the background begins to rise sharply. Despite an increase in noise due to the background increase, the CH_3 mode can still be observed as a broad hump until about 540 ns. After that, the spectra flatten out and no hump is discernible. However, the results of experiment 2 show that the CH_3 peak does not disappear. Rather, because of the higher spectral dispersion in experiment 3, the broadening of the CH_3 peak renders it indistinguishable from the spectral fluctuations in the background.

Experiment 4 used the high dispersion configuration to observe the CN mode and the NO_2/CH_3 mode under conditions similar to those in experiment 3. The results are shown in Figure 6. With the increase in pressure, the shifting of both peaks to higher energy is evident, as is the simultaneous enhancement of the NO_2/CH_3 mode. After peak pressure is reached, the peaks change little until about 675 ns, when the CN mode undergoes a substantial softening, which lasts for about 225 ns. The NO_2/CH_3 mode does not display a similar softening. However, as peak pressure is reached, a shoulder appears on the low-energy side of the peak. The position of this shoulder remains constant for the duration of the experiment, with the shoulder becoming more distinct as time progresses. The background rise in this experiment is slow until about 600 ns, when it becomes more rapid. In contrast to the behavior of the CH_3 mode in experiment 3, the CN and NO_2/CH_3 modes exhibit little broadening. The two peaks remain clearly discernible throughout the duration of the experiment.

B. Unloading Experiment at T_0 = 298 K. Experiment 5, an unloading experiment, was performed to determine the reversibility of spectral changes that were observed in experiments 2−4. The pressure and temperature profiles at the center of the sample for experiment 5 are shown in Figure 7. In the recorded spectra, the background rose rapidly after peak pressure was reached, but the Raman peaks showed little change beyond the usual pressure-induced shift. At 400 ns, the unloading began and the unloading pressure of about 7.0 GPa was reached at 550 ns. The background was observed to drop dramatically as the unloading process occurred. This background drop is shown in Figure 7, where the time profile of the background level is compared with the time profiles of the pressure and temperature. Despite the rise and fall of the background, the Raman peaks were still well defined until about 630 ns, at which point the intensity of all three peaks began to drop due to an experimental artifact.

C. Stepwise Loading Experiments at T_0 > 298 K. Experiment 6 was performed to distinguish the roles of temperature and pressure in the observed spectral changes. The results, despite the difference in peak pressure, were very similar to those of experiment 2. As in experiment 2, the background increased slowly until about 585 ns after the shock reached the sample. At this point, the background rose sharply and the CH_3 stretching mode began to broaden somewhat, although the extent was not as great as in experiment 2. The behavior of the CN mode became somewhat obscured by noise as the background increased. The enhancement of the NO_2/CH_3 mode with pressure was apparent but less pronounced than that in Experiment 2, perhaps due to the lower pressure.

Experiment 7 was performed to examine the behavior of the Raman peaks at higher pressures and temperatures. The results, for selected times, are displayed in Figure 8. After peak pressure is reached, the background begins to rise. At about 405 ns, the background begins to rise very rapidly. At 495 ns, the CH_3 peak undergoes extreme broadening and the CN peak softens.

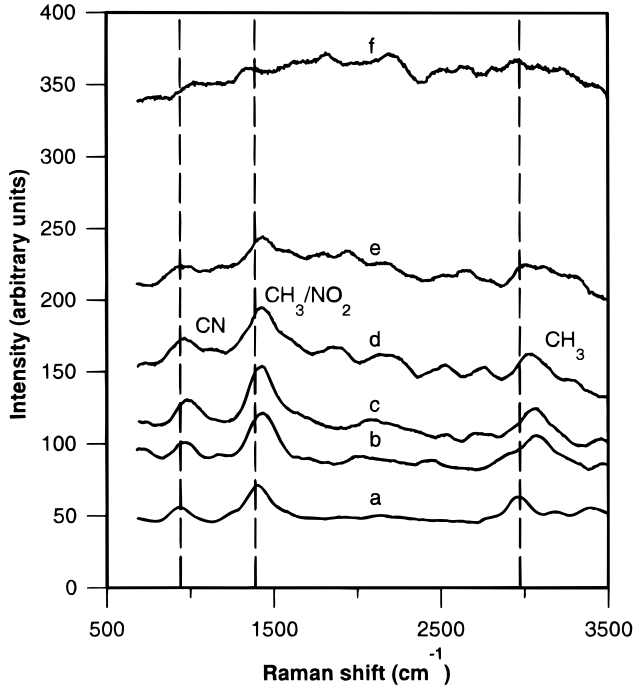

Figure 8. Selected Raman spectra of NM shocked to 16.8 GPa (experiment 7). Initial temperature = 322 K, peak temperature = 980 K. Time relative to the when the shock wave reached the sample: (a) 0 ns, (b) 270 ns, (c) 360 ns, (d) 450 ns, (e) 495 ns, (f) 540 ns. The vertical lines mark the positions of the peaks at ambient pressure. Peak pressure was attained at 270 ns.

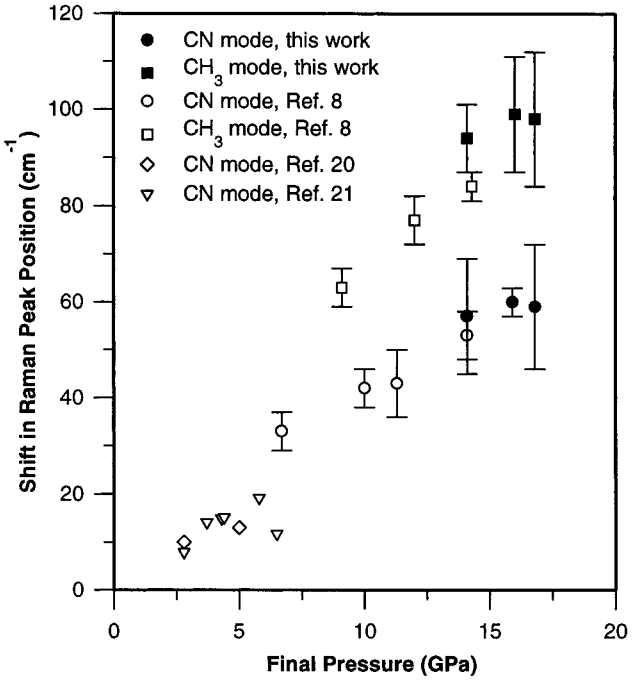

Figure 9. Shock-induced change in Raman frequency versus final pressure.

By 540 ns, the peaks have all fallen below noise levels and are not discernible.

IV. Discussion of Results

The discussion of the results is presented in several parts: A discussion of spectral changes occurring only during the reverberation time of the stepwise loading is given first. These changes remain constant as long as the sample remains at peak pressure. Next, a discussion is given of spectral changes which occur after peak pressure is reached. These changes are related to the onset of reaction in the sample. This discussion is followed by an examination of previously proposed mechanisms of decomposition and a comprehensive interpretation of the experimental results.

To analyze the data, Gaussian functions were fitted to the Raman peaks and a polynomial function was fitted to the background. This yielded information on the peak positions, peak widths, and peak intensities as functions of time. The peak widths shown in the figures are not the natural widths of the modes since the natural peaks were convoluted with the instrument response profile. To extract the natural widths from the data, the peaks were deconvoluted by approximating both the instrument response profile and the natural peak shape with Gaussian functions. Since the measured peak shape was fitted with a Gaussian function, the square of the measured peak width was equal to the sum of the squares of the widths of the instrument response profile and the natural peak shape. Therefore, knowing the width of the instrument response, the natural peak width could be calculated.

A. Spectral Changes Occurring Only during the Shock Reverberation Time. These changes are best observed in the data (Figure 2) from experiment 1, since there is little change in the spectra after peak pressure is reached. Two significant effects can be identified in these results: the pressure-induced shifting of the Raman peaks to higher vibrational frequency and an enhancement of the NO_2/CH_3 peak.

1. Shock-Induced Shift of the Raman Peaks. In every experiment, the Raman peaks shifted to higher vibrational frequency with increasing pressure. This effect has been observed in earlier work on shocked NM.[8,20,21] The shock-induced shifts of the CN and CH_3 symmetric stretching modes at final pressure are plotted against final pressure in Figure 9. Earlier results of other workers are also plotted for comparison. The data for the NO_2/CH_3 peak were not plotted because the interpretation of the results for these overlapped peaks is not straightforward. The shock-induced changes in Raman frequency for each peak were obtained by comparing the average position of the Raman peak before the shock reached the sample with the average position after final pressure was reached. The uncertainty in the shock-induced shift of the Raman peaks was determined from the standard deviations of these averages.

In Figure 9, the data for the CN peak from the present work and from ref 8 show a consistent trend toward higher vibrational frequencies with increasing pressure. The shift of the CH_3 peak in the present work appears to be somewhat larger than the corresponding shifts for the data in ref 8. However, the large error bars in our data prevent definite conclusions from being drawn. The larger error bars, compared to those in ref 8, are due to the lower spectral resolution in the experiments reported here. The data from refs 20 and 21, which were taken under single shock loading conditions, do not correlate well with either the data from the present work or the data from ref 8. However, the data of refs 20 and 21 were the result of preliminary efforts and the error bars are not known. Therefore, these earlier data should be viewed with caution.

As noted previously,[8] the observed frequency shifts in NM are quite large, compared to the pressure-induced shifts in other materials, suggesting the presence of strong, shock-induced, intermolecular interactions. Because of the low mass of the hydrogen atoms and the position of these atoms on the periphery of the NM molecule, the CH_3 mode should be the most sensitive to intermolecular interactions. The larger shift in the CH_3 mode, compared to earlier observations,[8] therefore suggests that the

shock-induced intermolecular interactions are at least as strong, possibly stronger, at higher shock pressures and temperatures.

2. Shock-Induced Enhancement of the NO_2/CH_3 Peak. An enhancement of the NO_2/CH_3 peak with increasing pressure was observed consistently in our experiments. This pressure-induced enhancement was observed previously[8] and was discussed in terms of a resonance Raman effect. However, the selective enhancement of the NO_2/CH_3 peak, relative to that of the other peaks, was not explained.

In experiment 4 (Figure 6), a shoulder appeared on the low-energy side of the NO_2/CH_3 peak as final pressure was reached. Since the CH_3 symmetric bending mode was previously assigned the lower energy of the two unresolved modes[12] and since the position of the shoulder coincides with the ambient pressure position of the CH_3 bend,[12,14] the shoulder is assigned to the CH_3 bending mode. This assignment is supported by the fact that bending modes involving A−H bonds are much less sensitive to intermolecular interactions than A−H stretching modes.[22] Therefore, A−H bending modes exhibit a much smaller pressure-induced frequency shift. With this assignment, it is clear from Figure 6 that the pressure-induced enhancement of the NO_2/CH_3 mode is due primarily to enhancement of the NO_2 stretching mode, rather than the CH_3 bending mode. This is evident from the fact that, under shock conditions, the intensity of the NO_2 stretch is larger than that of the CH_3 bend by a factor of 3 (Figure 6), whereas at ambient pressure the NO_2 stretch and the CH_3 bend are of comparable intensity.[13]

Because the NO_2 symmetric stretching mode has been related previously to observed resonance Raman effects,[23] it is reasonable to think of the NO_2 enhancement observed here as a resonance Raman effect as well. Since a shock wave causes a substantial red-shift of the band edge of the n−π* absorption band of NM,[9,11] it is plausible that this shock-induced shift in the band edge could cause a small amount of absorption at the 514.5 nm laser line. The band edge itself would not have to be very close to the laser line to account for the effect, since the observed enhancement in the Raman peak is not large.

The fact that modes other than the NO_2 symmetric stretch are not enhanced serves to strengthen the argument. It is known that only those modes which are localized in the chromophoric part of the molecule will be resonantly enhanced.[24] Since the highest occupied molecular orbital (HOMO) and the lowest unoccupied molecular orbital (LUMO) of NM are both localized on the NO_2 group,[25] the NO_2 group is the chromophore for the HOMO−LUMO (n−π*) transition. The CN and CH_3 modes would, therefore, not be expected to show significant enhancement. Furthermore, the modes which show the strongest resonance enhancement are those causing molecular distortions which are most similar to the distortions caused by the electronic transition to the excited state.[24] The n−π* transition produces a transition from a nonbonding orbital of the NO_2 group to an antibonding orbital of the NO_2 group.[25] This would tend to lengthen the two NO bonds in a symmetric way, without producing a large amount of change in the O−N−O bond angle. Therefore, it is not unexpected that the NO_2 symmetric stretching mode is enhanced while the NO_2 scissors mode and the NO_2 anti-symmetric stretching mode are not.

B. Spectral Changes Occurring After Peak Pressure Is Reached. The spectral changes occurring after peak pressure is reached include changes in the background as well as changes in the Raman peaks. These changes occur well before the end of the induction time as measured in previous absorption experiments.[11] For a peak pressure of 16 GPa and a peak temperature of 910 K, the absorption induction time is calculated to be about 2 μs by extrapolation of the analyzed absorption results.[11] Since the total duration of the Raman experiments is about 900 ns from when the shock enters the sample, the Raman data probe the high-pressure, high-temperature response of the NM sample during the induction time and well before the reaction is observed in the absorption data.

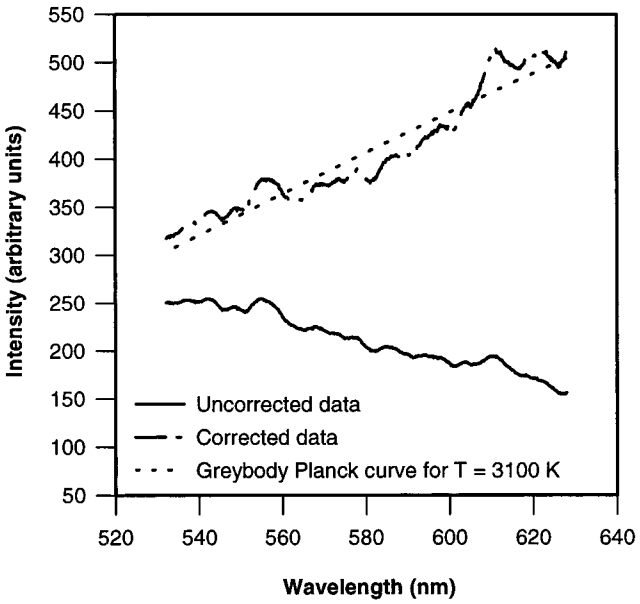

Figure 10. Spectral profile of the reaction-induced background (experiment 2). The solid curve is the uncorrected spectrum corresponding to 900 ns after the shock wave reached the sample. The dashed curve is the spectrum at 900 ns corrected for the spectral response of the instruments. The dotted curve is a fit of the graybody Planck distribution to the corrected data.

1. Spectral Background—A Probe of Reaction. An abrupt rise in background was observed in most of the Raman experiments. The effect is seen clearly in the spectra shown in Figure 3. This background rise is not caused by the effects of stepwise loading, either in the sample or in the cell windows, since it occurs well after peak pressure is reached. The rising background is therefore attributed to optical emission due to chemical changes in the NM sample.

Since this observation of reaction occurs prior to the end of the induction time in previous absorption experiments,[11] the Raman experiments are evidently a more sensitive probe of reaction. This results from the fact that small amounts of light emission are easier to detect than small amounts of absorption.

In experiment 6, a background rise with a similar onset time to that of experiment 2 was observed. The two experiments reached a similar peak temperature but experiment 6 reached a lower peak pressure. The similarity of the results in experiment 6 and experiment 2 suggests that in the Raman experiments reported here, as in the previous absorption experiments,[11] the peak temperature is the important parameter in initiating reaction.

To further investigate the cause of the reaction-induced background increase, the Raman spectra of experiment 2 were corrected for the spectral sensitivity of the data collection system. The spectrum corresponding to 900 ns after the shock wave entered the sample is shown in Figure 10. Also presented are the same data corrected for the spectral response of the instruments. The significant difference in the spectral profile of the corrected data compared to that of the uncorrected data is evident in the figure. This difference arises primarily from the spectral response of the streak camera.

Since the background rise or emission is reaction-induced, it must come from one of two sources: luminescence from early stage reaction products or thermal radiation due to heat generated

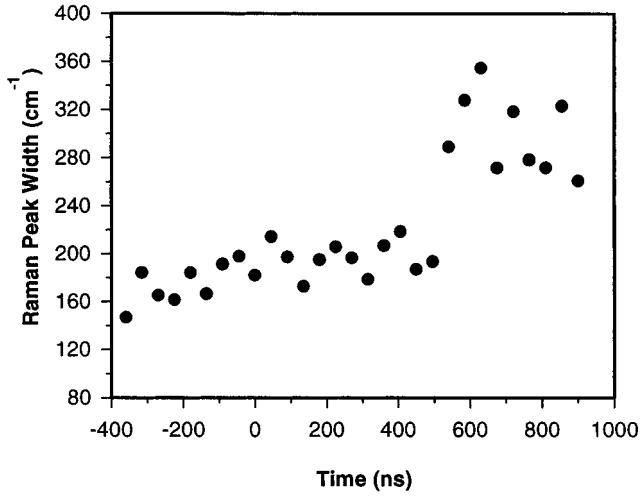

Figure 11. Width (fwhm) of the CH_3 peak vs time (experiment 2). Peak pressure = 16.1 GPa, peak temperature = 915 K. Time is relative to when the shock wave reached the sample.

by the reaction. While the background evidently peaks at a wavelength longer than 650 nm, which is a longer wavelength than many fluorescence bands, fluorescence or chemiluminescence from reaction products cannot be ruled out. In particular, the emission spectrum of NO_2 has broad fluorescence[26] and chemiluminescence[27−29] features that peak in the red or near-IR. Thermal radiation is an unlikely explanation for the background increase, because a fit of the graybody Planck distribution to the corrected background profile, shown in Figure 10, suggests a reaction-induced temperature of 3100 K. Since similar temperatures have been reported in detonating NM,[30,31] this temperature is unlikely for such an early stage of reaction. Hence, luminescence from reaction products seems to be the more plausible mechanism.

2. Peak Position and Width—Intermolecular Interactions. Significant changes in peak width and position are observed at final pressures of about 16 GPa. After peak pressure is reached, the spectral change that appears first is the broadening of the CH_3 stretching mode. Under high spectral resolution (experiment 3), the broadening occurs very rapidly after peak pressure is reached, as shown in Figure 5. With time, the peak becomes progressively broader until it is no longer visible above the noise levels. At later times, the broadening becomes extensive enough to be observed under low dispersion (experiment 2), as seen in Figure 4. Figure 11 shows the measured width of the CH_3 peak in experiment 2 as a function of time. The extreme broadening of the peak is clearly evident despite scatter in the data. The natural width of the broadened peak in experiment 2, after deconvoluting the peak from the instrument response profile, is estimated to be approximately 275 cm^{-1}.

Around the time when the CH_3 mode reaches its maximum width, the CN mode shifts to lower energy for a short period of time. This shift is observed under high dispersion (experiment 4), where it occurs without observable broadening. The shift of the CN peak as a function of time is shown in Figure 12. To facilitate comparison with events occurring in different experiments, time is shown relative to when peak pressure was reached. The transient nature of the CN shift is clearly observable in the figure. The timing of the CH_3 broadening from experiments 2 and 3 is also shown in Figure 12. From this comparison, the CN shift is shown to immediately follow the onset of extreme broadening of the CH_3 mode, observed in experiment 2 (Figure 4).

Also shown in Figure 12 is the pressure profile in the NM sample as calculated using the COPS wave propagation code.[18]

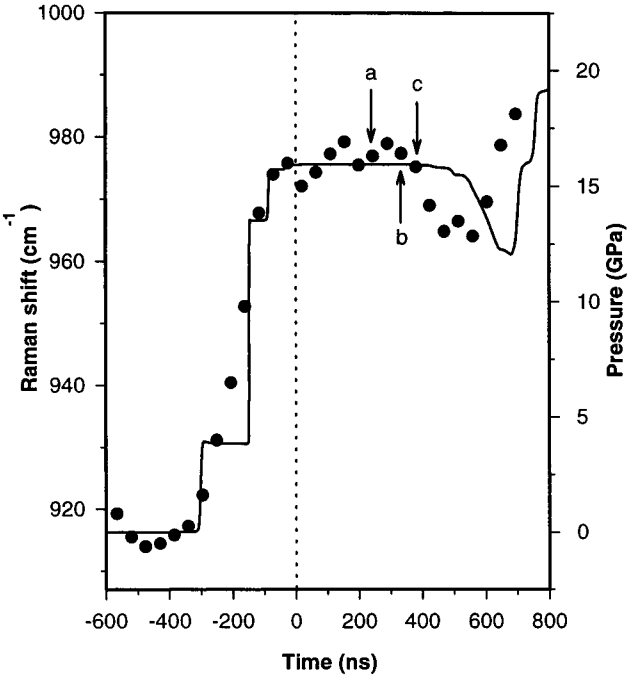

Figure 12. Position of the CN peak vs time (experiment 4). Peak pressure = 15.9 GPa, peak temperature = 910 K. Time is relative to when peak pressure was reached in the sample. The points are the CN peak position. The solid line is the calculated pressure history in the NM sample. The arrows mark the point in time when (a) the CH_3 peak disappears in experiment 3, (b) the CH_3 peak broadens dramatically in experiment 2, and (c) the CN peak softens in experiment 4.

This profile shows a substantial dip in the pressure, which occurs 150 ns after the transient shift in the CN mode. The transient release of pressure comes from a reflection of the initial shock wave at the interface of the LiF front window and the NM sample. The reflected wave traverses the LiF window, reflects off the sapphire impactor, and reenters the NM sample. The timing of this reentry thus depends on the mechanical response of the LiF window. Our LiF model in the COPS code is based on experimental data[32,33] characterizing the shock response of the material. The calculated arrival time of the transient release wave would have to be in error by approximately 20% to match the timing of the CN shift. An error of this magnitude in the wave velocity of LiF seems unlikely. Consequently, the CN shift is interpreted as mode softening due to molecular level changes in the sample, rather than the result of a transient release of pressure due to wave reflection. We present this interpretation with the caveat that our understanding of the transient softening of the CN mode remains incomplete. Our interpretation could be checked, in principle, by examining the shift in the NO_2/CH_3 peak from experiment 4, over the same time period, to look for a similar softening effect. Wave reflection would be expected to affect both the CN and NO_2/CH_3 peaks in a similar way. Unfortunately, the uncertainty in the position of the NO_2/CH_3 peak is sufficiently large that no conclusion can be drawn from the data.

As shown in Figure 8, broadening of the CH_3 mode is also observed at 16.8 GPa peak pressure in experiment 7, but it appears much earlier than in experiment 2. This is not unexpected, given the higher shock temperature in experiment 7, relative to experiment 2. Figure 8 also shows evidence of CN softening, simultaneous with massive broadening of the CH_3 mode, just before the peaks disappear. The broadening of the CH_3 mode is indicative of strong intermolecular interactions. It is well-known that intermolecular proton donor−acceptor interactions (such as hydrogen bonding) produce a substantial

amount of broadening in the stretching modes involving the proton donor.[34] In particular, the stretching modes of CH bonds that are involved in a hydrogen bond (C−H--O) are known to show broadening.[22,35] This is to be expected since these intermolecular interactions will occur between molecules of varying orientation and separation, thus creating inhomogeneous broadening due to the distribution in the strength of the interactions. The fact that the degree of broadening observed here increases with time indicates that the strength and extent of the intermolecular interactions also increase with time.

The softening of the CN mode indicates a weakening of the CN bond. However, despite the weakening of the bond, the lack of observable broadening in the CN peak precludes assignment of the softening to a dissociative reaction in the sample (i.e. CN bond scission). In view of the correlation in time with the extensive CH_3 broadening (Figure 12), a more reasonable interpretation is that the intermolecular interactions which cause the CH_3 broadening also produce a redistribution of charge within the NM molecule which serves to weaken the CN bond. Within this picture, the transient nature of the CN softening could then be explained by a reorientation of the molecules to a more energetically favorable intermolecular geometry. The ability of intermolecular interactions to influence the charge distribution in a molecule has been discussed in the literature.[36]

3. Intensity of Raman Peaks—Extent of Reaction. In the experiments with a peak pressure of approximately 16 GPa, there was no measurable loss in intensity of the Raman peaks within the experimental time window. This implies that, although the rising background indicated the onset of reaction in the sample, the extent of reaction was very small. Because Raman spectroscopy is not sensitive to changes involving small concentrations in the sample, the broadening of the CH_3 mode and the softening of the CN peak cannot be due to a reaction. Rather, these changes in the Raman peaks are due to effects occurring throughout the bulk of the sample and are, therefore, indicative of a precursor to reaction. These changes in the sample bulk occur during the induction time observed in previous absorption experiments.[11] Thus, the induction time is not characterized by a period of inactivity in the sample. Rather, it is a time period when the experimental probe (absorption measurement) is unable to detect any changes in the sample properties.

In Figure 7, the unloading of pressure is observed to bring about a rapid reduction in the background level. Since the background is directly associated with reaction, this result indicates that the reaction is quenched by the reduction of pressure and the accompanying reduction of temperature. As shown in Figure 7, the temperature drop due to unloading is relatively small (∼100 K) compared to the temperature increase due to multiple-shock loading. This is because the unloading occurs isentropically rather than through a multiple-shock process. That this small drop in temperature is sufficient to quench the reaction gives an indication of the strong temperature sensitivity (i.e. high activation energy) of the reaction, even after the reaction has been initiated.

A greater extent of reaction was observed at low dispersion at 16.8 GPa with an initial temperature of 322 K (experiment 7). As shown in Figure 8, around 450 ns after the shock enters the liquid, the peak intensities begin to drop rapidly. By 90 ns later, the peaks have disappeared below noise levels, which implies a reduction below $\sim^1/_3$ of their previous values. Thus, the reaction was quite extensive under these conditions. The timing of this peak loss (270 ns, relative to when peak pressure was reached) shows reasonable correlation with the loss of transmission in absorption experiments,[11] which were performed under similar conditions. This correlation comes from the fact that both the loss of Raman peaks and the loss of transmission indicate a substantial extent of reaction. Therefore, the timing of these observations should correlate better with each other than with an early reaction event like light emission.

This correlation between the loss of Raman peaks and the loss of transmission brings with it the possibility that the loss of the Raman peaks is in fact caused by attenuation of either the laser excitation or the Raman-scattered light. This possibility cannot be ruled out. However, in order for the reaction to generate absorbing species in sufficient concentration to attenuate the Raman signal, the extent of the reaction would still have to be large. The main conclusion derived from the loss of Raman peaks (namely, that the extent of reaction is large) is therefore unchanged by this interpretation.

C. Examination of Mechanisms. Proposed reaction mechanisms from the literature are examined, and the applicability of each mechanism to the data is discussed.

1. Unimolecular CN Bond Scission. Unimolecular CN bond scission has been proposed in connection with thermal decomposition work at relatively low pressures.[37,38] However, at higher pressures, this mechanism was not supported.[39−41] Likewise, in the present work, CN scission is not a favored mechanism. The early broadening of the CH_3 peak, given the lack of early changes in the CN peak, cannot be explained by this mechanism. The possibility does exist that CN scission could take place after the formation of an associative precursor state. However, this process would still be thermodynamically unfavorable at shock pressures, due to the nonnegative volume of activation for the reaction.[42,43]

2. Rearrangement to Methyl Nitrite. Based on thermal decomposition studies[44] and theoretical work,[45] it was proposed that NM could decompose by first undergoing a rearrangement to methyl nitrite (CH_3ONO). According to ab initio calculations on the reaction surface,[46] this rearrangement occurs most easily through scission of the CN bond of NM, followed by a recombination of the CH_3 and NO_2 radicals to form CH_3ONO. Shock wave experiments have suggested that methyl nitrite is more sensitive to shock-induced reaction than NM.[47] However, this mechanism still depends on the initial breaking of the CN bond, which is a thermodynamically unfavorable reaction at high pressures.[42,43] It also fails to account for the large amount of broadening in the CH_3 peak in the present experiments.

3. Aci-Ion Hypothesis. It has been demonstrated previously that the concentration of the nitromethyl aci-anion ($CH_2NO_2^-$) in NM is increased with the addition of certain sensitizing agents[48] and with the application of static high pressure.[49] This aci-anion was proposed as an important species in the shock decomposition of NM.[48] However, evidence for an increase in concentration of the aci-anion in neat NM under shock conditions has been found lacking.[20,50] Furthermore, the importance of the aci-anion in the sensitizing of NM by amines has been disputed in thermal decomposition work[38] and in shock wave decomposition work.[9] In the present experiments, the extensive broadening of the CH_3 peak could conceivably be explained by pressure-induced deprotonation of the NM molecule. However, the aci-anion has a CN double bond, which has a higher vibrational frequency than the CN single bond found in NM.[51] Therefore, a significant degree of deprotonization in the sample should cause inhomogeneous broadening of the CN peak as electronic charge is redistributed to the CN bond of interacting molecules. However, broadening of the CN peak is not observed.

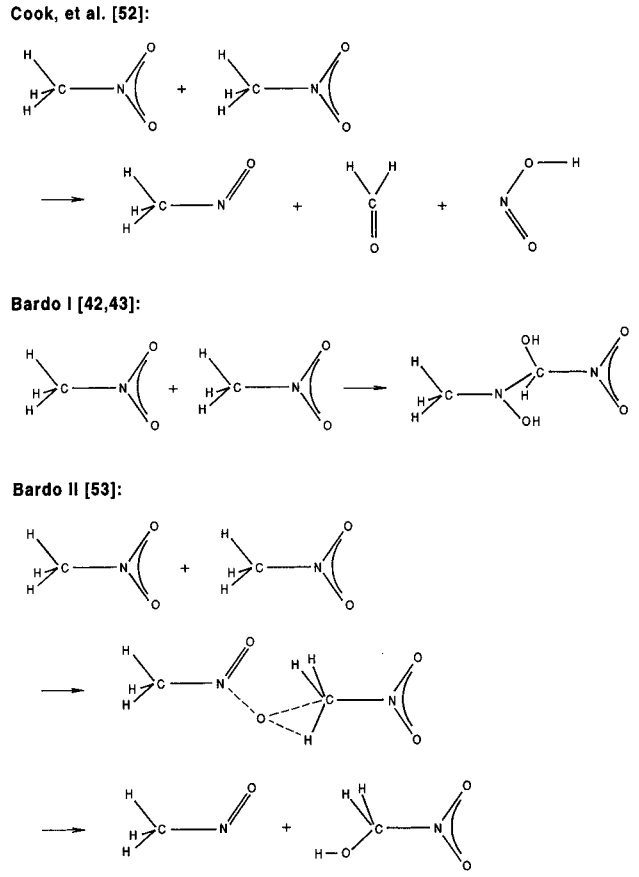

Figure 13. Bimolecular reaction mechanisms for nitromethane.

4. Bimolecular Mechanisms. In ab initio calculations, Cook et al.[52] have investigated a bimolecular mechanism with a strict head-to-tail geometry (CN bonds collinear). They found that the first reaction step resulted in the simultaneous production of nitrosomethane, formaldehyde, and HONO (Figure 13). The activation energy for this reaction was unrealistically high (119 kcal/mol), but this was probably due to the highly constrained geometry used in the calculations.

Two other bimolecular mechanisms have been proposed by Bardo[42,43,53] (Figure 13). The first of these models (Bardo I) involves an association reaction joining two NM molecules in a rearranged dimer.[42,43] This reaction is quite logical in light of the strong intermolecular interactions indicated by the broadening of the CH_3 peak. In addition, the kinetic parameters of the reaction are consistent with the time scales of shock initiation.[42,43] However this mechanism, as developed by Bardo, does not provide a direct pathway to the production of broadband absorbing species. The loss of transmission observed in previous absorption experiments[11] is therefore unaccounted for.

The second of Bardo's models (Bardo II) involves the bimolecular exchange of an oxygen atom to form nitrosomethane and nitromethanol[53] (Figure 13). This head-to-tail reaction is consistent with the broadening of the CH_3 peak and has activation parameters which are similar to the Bardo I mechanism.[42,43,53] In addition, the CN bond of nitromethanol is expected to be rather weak, leading to rapid CN scission and the formation of NO_2. The NO_2 radical is known to absorb over large regions of the visible spectrum,[54] and broadband fluorescence due to 514.5 nm excitation has been previously observed.[26] The radical has also been associated with broadband chemiluminescence at long wavelengths.[27−29] Thus, the formation of NO_2 could account for both the rising background in the Raman experiments (which use 514.5 nm excitation) and the loss of transmission in prior absorption experiments.[11] The Bardo II mechanism is therefore adopted to explain the shock-induced decomposition of neat NM.

D. Comprehensive Interpretation of the Experimental Results. Here, the data are shown to be consistent with an explanation which involves the development of strong intermolecular interactions which lead to intermolecular associations and a bimolecular reaction. In the Raman experiments reported here, intermolecular interactions are indicated almost immediately after peak pressure is reached through the broadening of the CH_3 peak (Figure 5). The progressive broadening of the CH_3 peak, seen in Figures 4, 5, and 10, indicates a progressive growth in the strength and extent of these intermolecular interactions. The fact that the CH_3 peak is most strongly affected suggests that the interactions occur through hydrogen bonding.[22,34,35] Almost immediately after the CH_3 peak reaches maximum broadening, the CN peak softens temporarily (Figure 12). The softening of the CN peak, given the lack of observable broadening or loss of Raman intensity (Figure 6), cannot be explained by dissociative reaction. Instead, it is most likely a manifestation of an increasing degree of association between molecules, in accordance with the increase in CH_3 broadening. The CN bond would thus be weakened through a redistribution of charge within the molecule caused by the intermolecular interactions. The transient nature of the CN softening is more difficult to explain. However, it could be indicative of a reorientational effect leading to a more highly ordered physical state. This is not unreasonable since the degree of CH_3 broadening suggests a hydrogen-bonding interaction involving the CH_3 group of one molecule and the NO_2 group of the other. This type of interaction is expected to be highly orientation dependent.[22] Theoretical work[55] has suggested that a side-by-side dimer (dipoles antiparallel) would be energetically favored over a head-to-tail dimer (dipoles aligned). However, a head-to-tail interaction geometry is favored here due to the known tendency of shock waves to cause alignment of dipoles in neat NM.[50,56,57] The higher pressure/temperature ratios achieved by the stepwise loading process in the present experiments, relative to the single-shock loading in refs 50 and 56, are expected to inhibit the relaxation of this dipole alignment.

Ab initio calculations have been performed for a system of three NM molecules,[58] arranged in the geometry of the crystalline solid. These calculations suggest that the CN bond of the central molecule will actually be strengthened slightly by the presence of the other two molecules. However, these calculations were quite crude by current standards and only one orientational configuration was examined. In addition, there is no indication that associations in shock wave experiments must assume the geometry of the solid phase. Caution must therefore be exercised in drawing conclusions from these results.

Because the extensive broadening of the CH_3 peak and the softening of the CN peak occur before the extent of reaction in the NM becomes significant, these spectral changes are indicative of the formation of an associative precursor state prior to the reaction. This reaction precursor is formed during the induction period previously measured using absorption experiments.[11] Its formation characterizes the evolution of the state of the NM sample during the induction time. The reaction sequence that leads to the observed emission of light in the Raman experiments reported here and the observed loss of transmission in prior absorption experiments[11] is believed to initiate among associated molecules in this precursor state. The fact that the start of the rise in background precedes the changes in the Raman peaks in some experiments can be explained as arising from the reaction of molecules which are already in a

favorable orientation for association and reaction when the shock reaches them. They will therefore associate and react earlier than the bulk of the sample. Since our Raman system is very sensitive to optical emission, these reacting molecules, though few in number, are easily observed.

Thermal decomposition work under static high pressure has provided evidence for a bimolecular decomposition mechanism in solid-phase NM.[39−41] In addition, Bardo[43,53] has performed calculations of reaction half-lives for various types of reactions at shock pressures. He concluded that, due to significant retardation of the reaction rate by pressure, unimolecular mechanisms for shock-induced reaction would not be competitive with bimolecular mechanisms.

Given the evidence for an associative precursor state in the current work, a bimolecular reaction mechanism is favored by the results of these experiments as well. The mechanism that best accounts for these experimental results is the Bardo II mechanism,[53] shown in Figure 13. This mechanism produces nitrosomethane (CH_3NO) and nitromethanol ($CH_2[OH]NO_2$) through the exchange of an oxygen atom. This exchange would be facilitated by the associative precursor state (the proposed source of the CH_3 broadening and the CN softening). The nitromethanol product is expected to decompose rapidly, producing an NO_2 radical. This relatively long-lived radical could account for both the emission of light observed in the Raman experiments reported here and the loss of transmission observed in previous absorption experiments.[11] The Bardo II mechanism, together with the associative reaction precursor, therefore accounts for all the major features observed in recent spectroscopy experiments on shocked, neat NM.

V. Concluding Remarks

The Raman measurements presented here have provided insight into the molecular changes accompanying chemical decomposition in neat NM under stepwise loading. In particular, the primary conclusions are the following: (1) The onset of shock-induced chemical reaction was indicated by the appearance of a rapidly rising background signal. This rising background likely resulted from the luminescence of early reaction products. (2) Broadening of the CH_3 mode and softening of the CN mode suggest strong intermolecular interactions leading to a proposed reaction precursor involving head-to-tail intermolecular associations. (3) Decomposition of the precursor is proposed to occur through a bimolecular mechanism, put forward by Bardo,[53] where nitrosomethane and nitromethanol are formed as initial products. Decomposition of nitromethanol to form NO_2 can explain the rapidly rising background signals.

Previous work[2−6,11] has identified the induction time as an important parameter in understanding shock-induced reaction in neat NM. However, comparison of our Raman measurements with earlier absorption[11] and continuum[2−6] results shows that the induction time depends strongly on the experimental method used to measure the parameter. The induction time, as measured by a particular method, is not defined by a lack of changes in the sample properties. Instead, it is determined by the threshold of the experimental method for detecting these property changes.

Time-resolved Raman spectroscopy has proven to be a very useful tool for probing the initial stages of chemical reaction in shocked NM. However, this technique is sensitive primarily to initial changes in the sample bulk. Therefore, to confirm the mechanistic ideas presented here and to probe farther into the reaction sequence, additional experimental methods are needed. Given the rising background in the Raman experiments, time-resolved fluorescence spectroscopy is a particularly attractive approach. Theoretical work is also needed to assist in the interpretation of experimental results. In particular, ab initio simulations can be very useful in selecting mechanistic models.

In conclusion, progress is being made in understanding the mechanistic issues central to the shock-induced decomposition of neat NM. This progress, and the methods used to achieve it, are expected to be of significant benefit in understanding shock-induced reaction in other energetic materials. However, more experimental and theoretical developments are needed to fully solve this challenging problem.

Acknowledgment. Useful discussions with Drs. G. I. Pangilinan, Y. A. Gruzdkov, and C. P. Constantinou are gratefully acknowledged. D. Savage and K. Zimmerman are both thanked for their expert assistance in the experimental effort. Prof. G. E. Duvall is sincerely acknowledged for his important role in the development of the NM equation of state used in this work. This work was supported by ONR Grants N00014-90-J-1400 and N00014-93-1-0369. The enthusiastic interest of Dr. R. S. Miller is sincerely appreciated.

References and Notes

(1) See proceedings of the *First through Tenth Symposia (International) on Detonation*; Office of Naval Research: Arlington, VA, 1951−1993.
(2) Campbell, A. W.; Davis, W. C.; Travis, J. R. *Phys. Fluids* **1961**, *4*, 498.
(3) Voskoboinikov, I. M.; Bogomolov, V. M.; Apin, A. Ya. *Fiz. Goreniya Vzryva* **1968**, *4*, 45.
(4) Berke, J. G.; Shaw, R.; Tegg, D.; Seely, L. B. in *Fifth Symposium (International) on Detonation*; Office of Naval Research: Arlington, VA, 1970; p 237.
(5) Walker, F. E.; Wasley, R. J. *Combust. Flame* **1970**, *15*, 233.
(6) Hardesty, D. R. *Combust. Flame* **1976**, *27*, 229.
(7) Gupta, Y. M. *J. de Physique IV, Colloque C4* **1995**, *5*, C4−345.
(8) Pangilinan, G. I.; Gupta, Y. M. *J. Phys. Chem.* **1994**, *98*, 4522.
(9) Constantinou, C. P.; Winey, J. M.; Gupta, Y. M. *J. Phys. Chem.* **1994**, *98*, 7767.
(10) Gupta, Y. M.; Pangilinan, G. I.; Winey, J. M.; Constantinou, C. P. *Chem. Phys. Lett.* **1995**, *232*, 341. The conclusions drawn in this paper are no longer believed to be valid as discussed in Gupta, Y. M.; Gruzdkov, Y. A.; Pangilinan, G. I. Accepted for publication in *Chem. Phys. Lett.*
(11) Winey, J. M.; Gupta, Y. M. *J. Phys. Chem. B* **1997**, *101*, 9333.
(12) Hill, J. R.; Moore, D. S.; Schmidt, S. C.; Storm, C. B. *J. Phys. Chem.* **1991**, *95*, 3037.
(13) Malewski, G.; Pfeiffer, M.; Reich, P. *J. Mol. Struct.* **1969**, *3*, 419.
(14) Winey, J. M. Time-Resolved Optical Spectroscopy to Examine Shock-Induced Decomposition in Liquid Nitromethane. Ph.D. Dissertation, Washington State University, 1995.
(15) Winey, J. M.; Gupta, Y. M.; Casey, K. G. In *High-Pressure Science and Technology−1993*; Schmidt, S. C., Shaner, J. W., Samara, G. A., Ross, M., Eds.; AIP Press: New York, 1994; p 1563.
(16) Fowles, G. R.; Duvall, G. E.; Asay, J.; Bellamy, P.; Feistmann, F.; Grady, D.; Michaels, T.; Mitchell, R. *Rev. Sci. Instrum.* **1970**, *41*, 984.
(17) SHOCKUP code; Ogilvie, K. M.; Duvall, G. E.; Collins, R. (Washington State University, Pullman, WA, 1984), unpublished.
(18) COPS code; Gupta, Y. M. (Stanford Research Institute, Menlo Park, CA, 1976), unpublished.
(19) Winey, J. M.; Knudson, M. D.; Duvall, G. E.; Gupta, Y. M. Unpublished.
(20) Renlund, A. M.; Trott, W. M. in *Shock Compression of Condensed Matter−1989*; Schmidt, S. C., Johnson, J. N., Davison, L. W., Eds.; Elsevier Science Publishers B. V.: Amsterdam, 1984; p 875.
(21) Delpuech, A.; Menil, A. in *Shock Waves in Condensed Matter−1983*; Asay, J. R., Graham, R. A., Straub, G. K., Eds.; Elsevier Science Publishers B. V.: Amsterdam, 1984; p 309.
(22) Vinogradov, S. N.; Linnell, R. H. *Hydrogen Bonding*; Van Nostrand Reinhold Co.: New York, 1971; p 53.
(23) Phillips, D. L.; Myers, A. B. *J. Phys. Chem.* **1991**, *95*, 7164.
(24) Spiro, T. G.; Loehr, T. M. In *Advances in Infrared and Raman Spectroscopy, Volume 1*; Clark, R. J. H., Hester, R. E., Eds.; Heyden: New York, 1975; p 100.
(25) Jaffe, H. H.; Orchin, M. *Theory and Applications of Ultraviolet Spectroscopy*; John Wiley and Sons: New York, 1962; pp 182−3.
(26) Sakurai, K.; Broida, H. P. *J. Chem. Phys.* **1969**, *50*, 2404.
(27) Haugen, G. R.; Steinmetz, L. L. *Mol. Photochem.* **1979**, *9*, 473.
(28) Doherty, G.; Jonathan, N. *Discuss. Faraday Soc.* **1964**, *37*, 73.
(29) Levitt, B. P. *Discuss. Faraday Soc.* **1964**, *37*, 222.

(30) Yoo, C. S.; Holmes, N. C. In *High-Pressure Science and Technology−1993*; Schmidt, S. C., Shaner, J. W., Samara, G. A., Ross, M., Eds.; AIP Press: New York, 1994; p 1567.
(31) Voskoboinikov, I. M.; Apin, A. Ya. *Dokl. Akad. Nauk SSSR* **1960**, *130*, 804.
(32) Carter, W. J. *High Temp.−High Press.* **1973**, *5*, 313.
(33) Zimmerman, K. Private communication.
(34) Sushchinskii, M. M. *Raman Spectra of Molecules and Crystals*; Israel Program for Scientific Translations: New York, 1972; p 264.
(35) Joesten, M. D.; Schaad, L. J. *Hydrogen Bonding*; Marcel Dekker: Inc.: New York, 1974.
(36) Fliszar, S.; Minichino, C. *J. de Physique, Colloque C4* **1987**, *48*, C4−367.
(37) Constantinou, C. P. *Int. J. Chem. Kinet.* **1994**, *26*, 1151.
(38) Constantinou, C. P.; Mukundan, T.; Chaudhri, M. M. *Philos. Trans. R. Soc. London A* **1992**, *339*, 403.
(39) Lee, E. L.; Sanborn, R. H.; Stromberg, H. D. In *Fifth Symposium (International) on Detonation*; Office of Naval Research: Arlington, VA, 1970; p 331.
(40) Piermarini, G. J.; Block, S. Miller, P. J. *J. Phys. Chem.* **1989**, *93*, 457.
(41) Rice, S. F.; Foltz, M. F. *Combust. Flame* **1991**, *87*, 109.
(42) Bardo, R. D. In *Eighth Symposium (International) on Detonation*; Naval Surface Weapons Center: White Oak, MD, 1985; p 855.
(43) Bardo, R. D. *Int. J. Quantum Chem. Symp.* **1986**, *20*, 455.
(44) Brower, K. R. *J. Org. Chem.* **1988**, *53*, 3776.
(45) Dewar, M. J. S.; Ritchie, J. P.; Alster, J. *J. Org. Chem.* **1985**, *50*, 1031.
(46) McKee, M. L. *J. Am. Chem. Soc.* **1986**, *108*, 5784.
(47) Shaw, R. *Combust. Flame* **1973**, *21*, 127.
(48) Engelke, R.; Earl, W. L.; Rohlfing, C. M. *J. Chem. Phys.* **1986**, *84*, 142.
(49) Engelke, R.; Schiferl, D.; Storm, C. B.; Earl, W. L. *J. Phys. Chem.* **1988**, *92*, 6815.
(50) Nabatov, S. S.; Yakushev, V. V.; Dremin, A. N. *Fiz. Gor. Vzryva* **1975**, *11*, 300.
(51) Dollish, F. R.; Fateley, W. G.; Bentley, F. F. *Characteristic Raman Frequencies of Organic Compounds*; John Wiley and Sons: New York, 1974; p 41.
(52) Cook, M. D.; Fellows, J.; Haskins, P. J. In *Decomposition, Combustion, and Detonation Chemistry of Energetic Materials, Materials Research Society, Symposium Proceedings, Vol. 418*; Materials Research Society: Pittsburgh, 1996; pp 267−275.
(53) Bardo, R. D. In *Ninth Symposium (International) on Detonation*; Office of Naval Research: Arlington, VA, 1989; p 235.
(54) Herzberg, G. *Molecular Spectra and Molecular Structure, III. Electronic Spectra and Electronic Structure of Polyatomic Molecules*; Van Nostrand Reinhold Co.: New York, 1966.
(55) Burgina, E. B.; Baltakhinov; V. P.; Boldyreva, E. V.; Stoyanov, E. S.; Zhanpeisov, N. Y.; Zhidomirov, G. M. *J. Mol. Struct.* **1993**, *296*, 53.
(56) de Icaza-Herrera, M.; Presles, H. N.; Brochet, C. *Rev. Phys. Appl.* **1978**, *13*, 547.
(57) Antipenko, A. G.; Dremin, A. N.; Yakushev, V. V. *Fiz. Goreniya Vzryva* **1978**, *14*, 101.
(58) Odiot, S.; Blain, M.; Vauthier, E.; Fliszar, S. *J. Mol. Struct. (THEOCHEM)* **1993**, *279*, 233.